Article

Cell Reports

Two Functionally Distinct Sources of Actin Monomers Supply the Leading Edge of Lamellipodia

Graphical Abstract

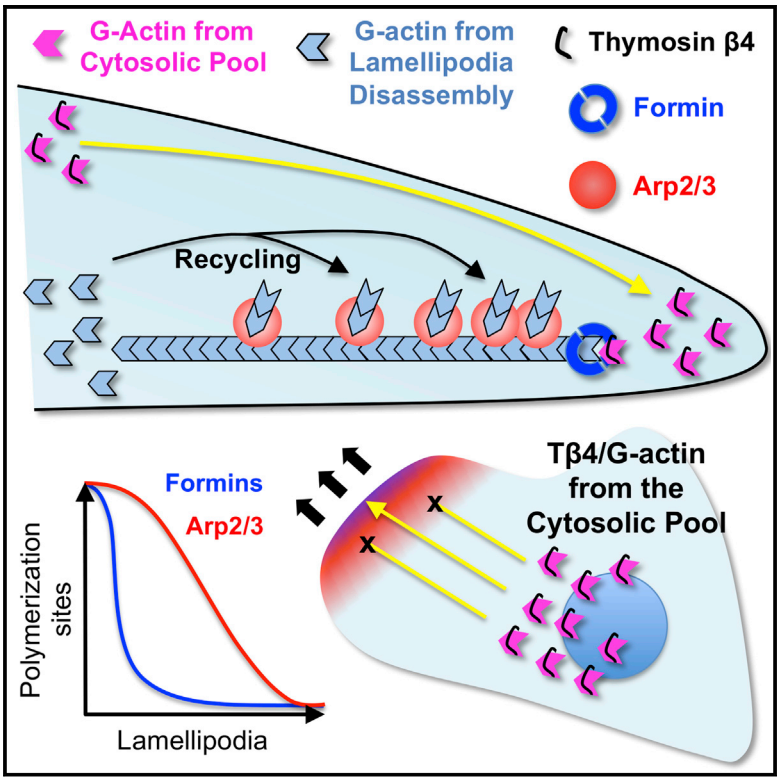

Authors

Eric A. Vitriol, Laura M. McMillen, ..., Dimitrios Vavylonis, James Q. Zheng

Correspondence

evitriol@ufl.edu (E.A.V.), james.zheng@emory.edu (J.Q.Z.)

In Brief

Vitriol et al. use quantitative live-cell imaging to show that lamellipodial actin networks are composed of actin monomers from two discrete subcellular pools.

Highlights

- Leading-edge G-actin comes from recycled lamellipodia F-actin and a cytosolic pool
- Cytosolic G-actin requires thymosin β4 for optimal leading-edge localization
- Cytosolic G-actin is predominantly targeted to formins at the leading edge
- Thymosin β4 prevents G-actin from binding to Arp2/3 polymerization sites

Vitriol et al., 2015, Cell Reports *11*, 433–445
April 21, 2015
http://dx.doi.org/10.1016/j.celrep.2015.03.033

CellPress

Cell Reports
Article

Two Functionally Distinct Sources of Actin Monomers Supply the Leading Edge of Lamellipodia

Eric A. Vitriol,[1,8,*] Laura M. McMillen,[2] Maryna Kapustina,[3] Shawn M. Gomez,[4,5] Dimitrios Vavylonis,[2] and James Q. Zheng[1,6,7,*]
[1]Department of Cell Biology, Emory University School of Medicine, Atlanta, GA 30322, USA
[2]Department of Physics, Lehigh University, Bethlehem, PA 18015, USA
[3]Department of Cell Biology and Physiology, University of North Carolina at Chapel Hill, Chapel Hill, NC 27599, USA
[4]Department of Computer Science, University of North Carolina at Chapel Hill, Chapel Hill, NC 27599, USA
[5]Department of Pharmacology, University of North Carolina at Chapel Hill, Chapel Hill, NC 27599, USA
[6]Department of Neurology, Emory University School of Medicine, Atlanta, GA 30322, USA
[7]Center for Neurodegenerative Diseases, Emory University School of Medicine, Atlanta, GA 30322, USA
[8]Present address: Department of Anatomy and Cell Biology, University of Florida, Gainesville, FL 32610, USA
*Correspondence: evitriol@ufl.edu (E.A.V.), james.zheng@emory.edu (J.Q.Z.)
http://dx.doi.org/10.1016/j.celrep.2015.03.033

SUMMARY

Lamellipodia, the sheet-like protrusions of motile cells, consist of networks of actin filaments (F-actin) regulated by the ordered assembly from and disassembly into actin monomers (G-actin). Traditionally, G-actin is thought to exist as a homogeneous pool. Here, we show that there are two functionally and molecularly distinct sources of G-actin that supply lamellipodial actin networks. G-actin originating from the cytosolic pool requires the monomer-binding protein thymosin β4 (Tβ4) for optimal leading-edge localization, is targeted to formins, and is responsible for creating an elevated G/F-actin ratio that promotes membrane protrusion. The second source of G-actin comes from recycled lamellipodia F-actin. Recycling occurs independently of Tβ4 and appears to regulate lamellipodia homeostasis. Tβ4-bound G-actin specifically localizes to the leading edge because it does not interact with Arp2/3-mediated polymerization sites found throughout the lamellipodia. These findings demonstrate that actin networks can be constructed from multiple sources of monomers with discrete spatiotemporal functions.

INTRODUCTION

Lamellipodia of motile cells contain a stereotypic meshwork of branched actin filaments interspersed by parallel actin bundles (Svitkina, 2013). Lamellipodia actin networks constantly undergo rapid turnover but are typically maintained in size through rapid assembly at the leading edge and disassembly at the rear (Blanchoin et al., 2014). While estimates have varied and depend on cell type, it is agreed that G-actin is present in cells at a concentration that is orders of magnitude above the critical concentration for F-actin assembly (Pollard et al., 2000). This large reservoir of actin is maintained by the presence of sequestering co-factors, such as Tβ4 and Profilin, that allow for G-actin to be present at concentrations much higher than the critical concentration for actin polymerization in vitro without spontaneous polymerization. This large pool of unpolymerized actin has been considered to be the major, if not only, reservoir for all actin assembly. The finding that the concentration of G-actin is approximately the same in the F-actin-rich lamellipodia as it is in the cell body (Kiuchi et al., 2011) supports the idea that actin monomers exist as a single, contiguous source. Further, while the concept that lamellipodia disassembly of F-actin recycles actin back into the polymerization-competent monomer pool has been around for some time (Pollard et al., 2000; Pollard and Borisy, 2003), it has never been shown that this G-actin is recycled in the sense that it is more likely to return to the lamellipodia instead of any other type of actin structure. Recently, we demonstrated that there is a pool of G-actin that is dynamically localized to the leading edge in migrating cells during membrane protrusion (Lee et al., 2013), raising the question of whether these monomers may have been acquired from a specific fraction of the large G-actin pool and/or were under distinct molecular regulation that directed them to the leading edge. From a broader perspective, this would mean that multiple, discrete sources of actin monomers could be used to build and regulate a complex F-actin structure, like lamellipodia. In this study, we present evidence that the F-actin network of lamellipodia is constructed from two pools of G-actin that regulate distinct aspects of actin-based lamellipodial dynamics.

RESULTS

Incorporation of G-actin into the Leading Edge from the Cytosolic Pool

To examine whether a single or multiple sources of G-actin supply lamellipodial F-actin assembly, we used photoactivatable GFP-γ-actin (PA-GFP-actin) to pulse-label actin from different

regions of the cell and measured its incorporation into the lamellipodia actin network. Lifeact, a small F-actin-binding peptide (Riedl et al., 2008) linked to the red fluorescent protein mRuby, was co-expressed in these experiments to highlight the F-actin cytoskeleton. We used Cath.a-differentiated neuroblastoma cells (CAD) (Qi et al., 1997) because their round shape after plating on a laminin substrate—with most, if not all, of the entire cell periphery consisting of lamellipodia—make them extremely amenable to automated, quantitative analysis. To ensure that photoactivation of PA-GFP-actin did not perturb actin dynamics at the leading edge, we photoactivated a region of the lamellipodia in PA-GFP-actin-expressing cells at varying laser powers and measured the clearance of PA-GFP fluorescence from that area, a process that reflects the assembly/disassembly of actin, since it is dependent on both polymerization-driven retrograde flow and F-actin depolymerization. There was no effect on actin clearance, even when the laser was at 100% (Figure S1A). Further, there was no relationship between the amount of PA-GFP-actin in lamellipodia (as represented by the initial fluorescence intensity using the same photoactivation laser power) and actin clearance (Figure S1B). Therefore, under our experimental settings, different laser powers and amounts of PA-GFP expression exert minimal effects on the actin dynamics in lamellipodia.

We hypothesized that, if there were spatially separate pools of G-actin that supply the leading edge, they would come from either the cytosolic pool via long-range transfer (Fan et al., 2012; Zicha et al., 2003) or a local pool generated from lamellipodial F-actin disassembly (Smith et al., 2013). For the cytosolic pool, we photoactivated PA-GFP-actin in the cell center, which included all parts of the cell except the lamellipodia (Figure 1A; Movie S1). Actin photoactivated here rapidly localized to the leading edge and became incorporated into the lamellipodial actin network (Figure 1A; Movie S1). In fact, within 60 s, approximately 40% of actin that originated at the cell center had left that region and incorporated into the actin network of the leading edge (Figure 1B). Therefore, G-actin from the cytosolic pool substantially contributes to the assembly of the lamellipodial F-actin network.

Incorporation of G-actin into the Leading Edge from Recycled Lamellipodia F-actin

Next, we photoactivated PA-GFP-actin in the lamellipodia to determine whether lamellipodial actin is recycled. It has been reported that actin photoconverted in the lamellipodia completely escapes the converted region through retrograde flow and depolymerization (Burnette et al., 2011; Lai et al., 2008), arguing against the notion of local actin recycling in the lamellipodia. However, an important feature of those experiments is that they were conducted by only photoconverting a small region of the lamellipodia. If recycling were taking place, one would expect that some fluorescence would be retained in the area of the lamellipodia that was initially highlighted. Consistent with previous studies (Burnette et al., 2011; Lai et al., 2008), photoactivating a sub-fraction of the lamellipodia (a region 10 μm × 5 μm) showed that, within 2 min, nearly all of the fluorescent actin from this region had left (Figures 1C and 1D; Movie S2). However, when we carefully scaled the PA-GFP-actin images to maximize small changes in intensity close to background levels (Figure 1C, inverted grayscale image sequence; Movie S2), two subtle features of the time-lapse sequence became apparent: photoactivated PA-GFP-actin began to spread to the leading edge immediately adjacent to the photoactivated region (Figure 1C, blue arrowheads), and a small amount of fluorescence persisted in the initial segment of the lamellipodia that was highlighted (Figure 1C, red arrowheads) as the bulk of the photoactivated actin moved rearward by retrograde flow. These observations indicate that local actin recycling may be occurring and that, in order to see it clearly, one would have to visualize turnover of the cell's entire lamellipodia.

We then selectively photoactivated the cell's entire lamellipodia (Figure 1E; Movie S3) and measured the fluorescence of PA-GFP-actin in a 1-μm-wide band at the leading edge (Movie S4). After the actin that was initially localized there had moved rearward by retrograde flow, we observed that leading-edge PA-GFP-actin fluorescence values stabilized at approximately 50% of the initial value and remained there for over 2 min (Figures 1E and 1F; Movie S3). With a retrograde flow rate of approximately 70 nm/s (see Figure S2), actin that incorporated at the edge would move rearward through this 1-μm-wide region every 14 s, meaning that the 2-min observation period represents over eight complete turnover cycles for this region.

One potential explanation for the ~50% plateau in fluorescence intensity at the leading edge is that half of the cell's actin is contained in the lamellipodia, and the stabilization of intensity values simply represents the cell reaching an equilibrium in actin between the lamellipodia and the rest of the cell. To exclude this possibility, we performed experiments where we drew a photoactivation region of interest (PA ROI) that represented half of the cells' total area, taking care to pick cells that were symmetric in a manner that allowed bisection through the nucleus (where PA-GFP-actin is excluded) and that the PA ROI and the non-photoactivated region both contained approximately one half of the cell's lamellipodia and cytosolic compartments (Figure 1H). In experiments where we photoactivated the entire lamellipodia, fluorescence intensities plateaued at ~50% in 20 s. In experiments where we photoactivated half of the cell's total area, after 20 s, the PA ROI had only lost approximately 10% of its initial intensity (Figure 1I). Even after 80 s, the fluorescence loss was only 25% (Figure 1I), demonstrating that the timescale that it takes for the cell to reach equilibrium after 50% of its actin is photoactivated is too slow to explain our whole-lamellipodia photoactivation experiments and indicates that the plateau in fluorescence values there represents a reintroduction of G-actin to the leading edge from the existing lamellipodia F-actin.

Additionally, we stained cells with fluorescently labeled phalloidin and measured the percentage of F-actin that was present in the lamellipodia. We found that, on average, only 32% ± 4% (95% confidence intervals, n = 11) of cells' total F-actin was found there at any given time. Taking into account that the cell has roughly equimolar amounts of G- and F-actin, this would mean that only approximately 10%–20% of the total actin is in the lamellipodia. Thus, we believe that lamellipodia recycling does occur and is responsible for a substantial amount of the actin that is incorporated into the leading edge at steady state. Further, one additional feature of the image sequences from whole-lamellipodia photoactivation experiments was that there was a dark band that appeared in the highlighted region, signifying actin

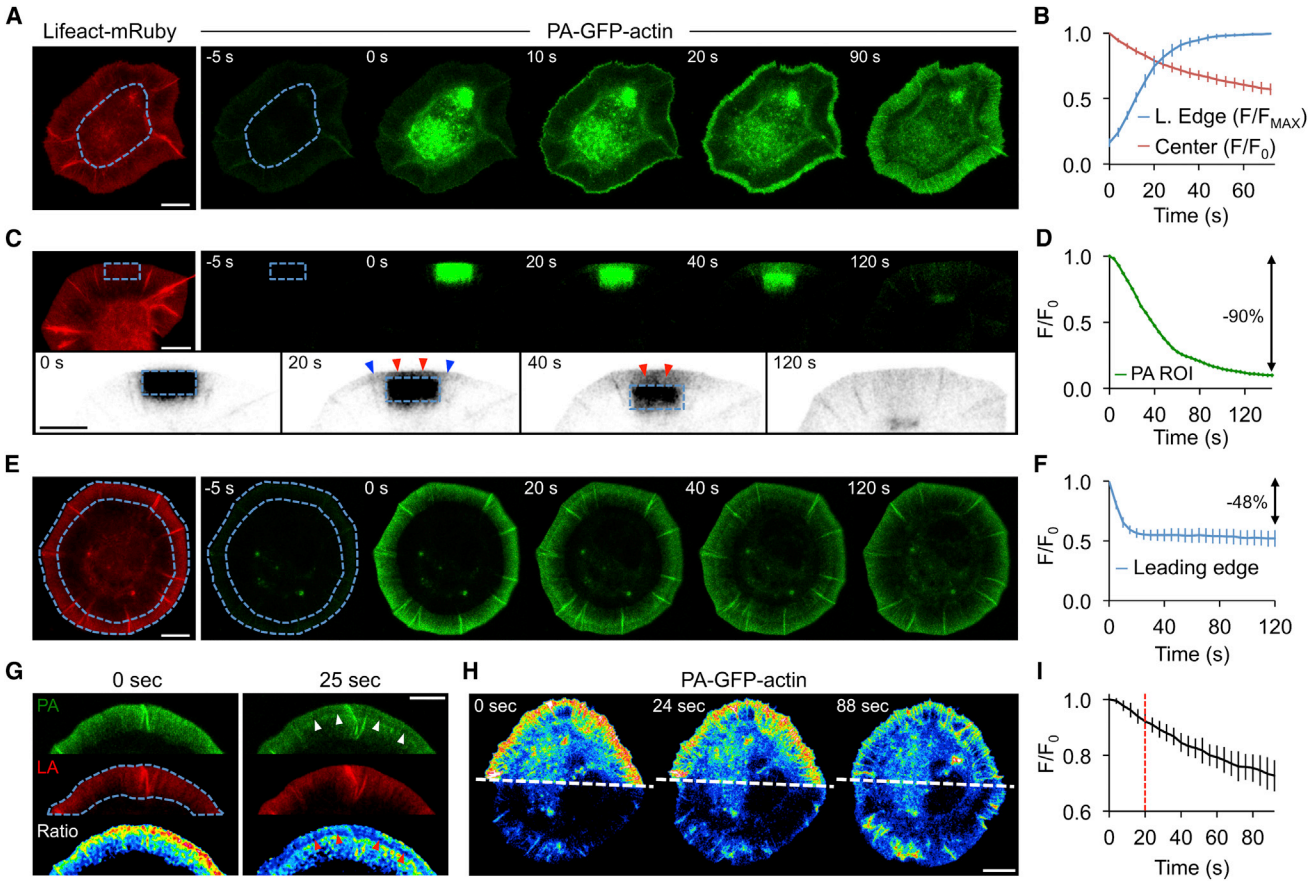

Figure 1. Identification of Two Distinct Subcellular Sources of G-actin Used to Make the Lamellipodia

(A–C) To determine whether actin monomers that incorporated into the lamellipodia actin network come from a specific subcellular source, PA-GFP-actin (green) and Lifeact-mRuby (red) were co-expressed in cells. Specific regions were highlighted by PA-GFP photoactivation and then followed over time (shown in seconds after photoactivation). (A) PA-GFP-actin was selectively photoactivated in the cell center (shown by dotted blue line). This region included all parts of the cell F/except the lamellipodia. (B) Line graph showing the average decrease of fluorescence in the cell center (F/F_0) and increase in fluorescence in at the leading edge (F_{MAX}) following photoactivation of PA-GFP-actin in the cell center. (n = 14 cells). (C) PA-GFP-actin was selectively photoactivated in partial region of the lamellipodia. Enlarged, inverted grayscale versions of the PA-GFP-actin images are shown in the inset. The blue arrowheads highlight PA-GFP-actin that has localized to the leading edge outside of the PA ROI. The red arrowheads highlight PA-GFP fluorescence that has remained in the photoactivated region after the actin has been moved rearward by retrograde flow. F, current time point; F_0, first time point; F_{MAX}, time point with highest intensity.

(D) Line graph showing the decrease of fluorescence at the leading edge (F/F_0) following partial photoactivation of PA-GFP-actin in lamellipodia. This graph is from the cell shown in (B).

(E) PA-GFP-actin was selectively photoactivated in the entire lamellipodia.

(F) Line graph showing average fluorescence loss at the leading edge of the lamellipodia following photoactivation of the entire lamellipodia (n = 12 cells).

(G) Representative images show PA-GFP-actin (PA, top panels), Lifeact-mRuby (LA, middle panels), and the actin/Lifeact ratio (bottom panels) for a cell in which PA-GFP-actin was photoactivated in the lamellipodia 0 and 25 s after photoactivation. Arrowheads highlight a decrease in fluorescence in the PA-actin and actin/Lifeact ratio panels caused by actin outside of the photoactivated region being incorporated into the lamellipodia.

(H) Representative images show a cell 0, 24, and 88 s after photoactivation of PA-GFP-actin, where the PA ROI contained half of the cell's total area and the cell was bisected in such a way where both the PA ROI and the non-photoactivated region both contained approximately one half of the cell's lamellipodia and cytosolic actin pools. The images have been scaled identically and psuedocolored to visualize relative changes in fluorescence intensity.

(I) Line graph showing the average relative change in fluorescence intensity after photoactivation of PA-GFP-actin in the PA ROI (n = 7).

All error bars represent 95% confidence intervals. Image scale bars are 10 μm.

localizing to the leading edge that was not part of the photoactivated group (Figure 1G; Movie S3). This demonstrates that actin incorporation from the cytosolic pool and from recycled filaments occurs simultaneously and hints that the balance between the two pathways may be a way to regulate leading-edge behavior. However, to be considered separate pathways, they must be under distinct molecular regulation.

Tβ4 Specifically Enhances the Localization of Cytosolic G-actin to the Leading Edge

Previously, we have identified Tβ4 as an essential factor in creating the high G-actin/F-actin ratio at the leading edge of protruding lamellipodia (Lee et al., 2013), presumably by localizing monomers there (Fan et al., 2009, 2012). We used our photoactivatable actin assays to determine whether Tβ4 is responsible

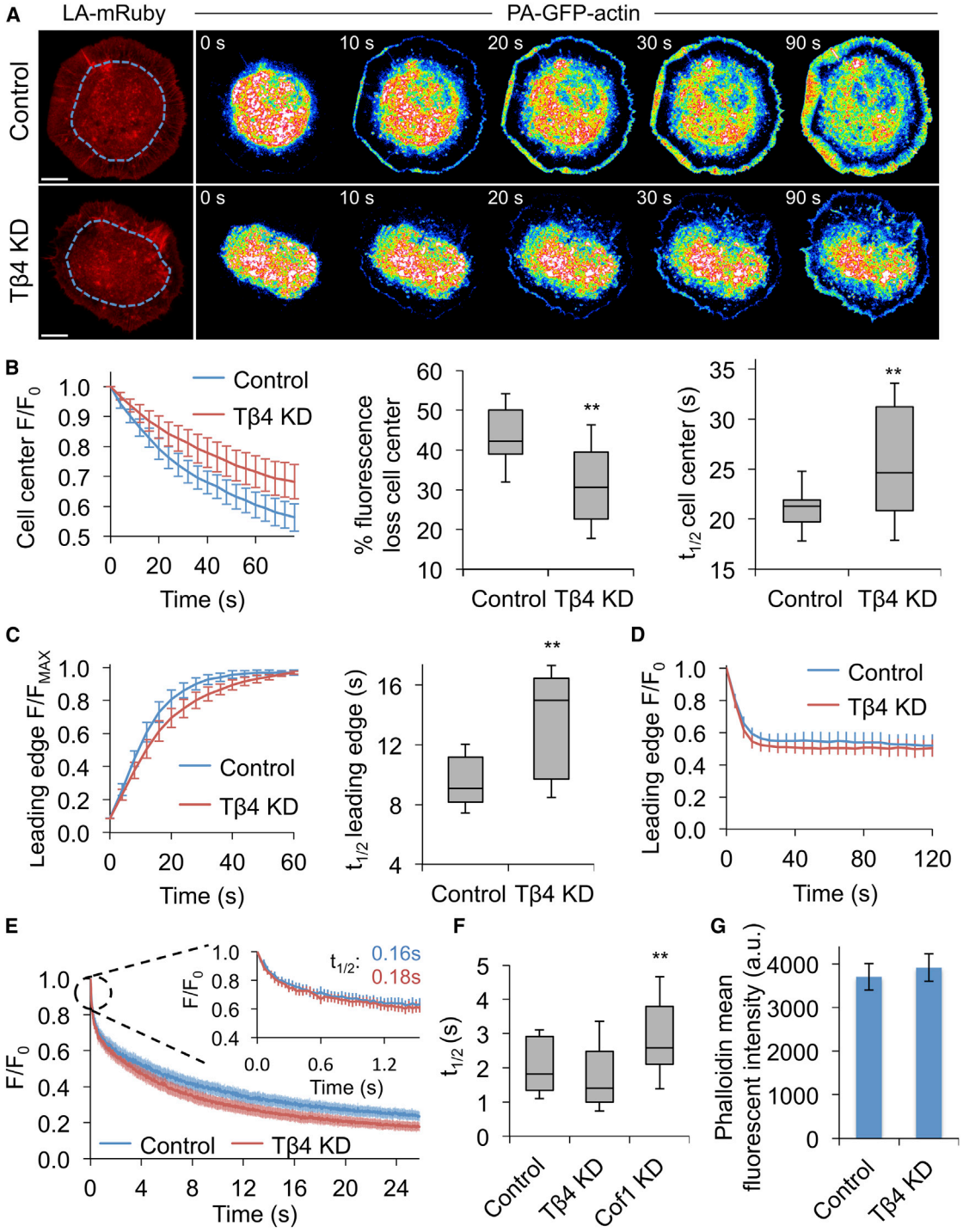

Figure 2. The Two Pools of Actin that Contribute to the Leading Edge Are Molecularly Distinct

(A) Representative images from a time lapse where PA-GFP-actin was photoactivated in the cell center (shown by dotted blue line) for cells expressing a scramble shRNA1 (Control) or an shRNA for Tβ4 (Tβ4 KD). PA-GFP-actin images were scaled identically and pseudocolored to visualize changes in fluorescence intensity. (B and C) Experiments where actin was photoactivated in the cell center. (B) The line graph shows the average fluorescence intensity loss at the cell center (left) for both control (n = 14) and Tβ4 KD cells (n = 17). The box-and-whisker plots depict the average fluorescence loss at the cell center (left), the $t_{1/2}$ for fluorescence loss at the cell center from these experiments. (C) The line graph shows the increase in fluorescence intensity at the leading edge. The box-and-whisker plot depicts the $t_{1/2}$ for fluorescence gain at the leading edge for both control (n = 13) and Tβ4 KD (n = 16) cells.

(legend continued on next page)

for localizing actin from the cytosolic pool, the lamellipodia recycling pathway, or both to the leading edge. In the assay where actin is photoactivated in the cell center, cells expressing a short hairpin RNA (shRNA) against Tβ4 (Tβ4 knockdown [KD]) exhibited a substantial inability to move actin away from the cell center (Figures 2A and 2B) relative to control cells expressing a scramble shRNA. Additionally, they incorporated actin more slowly into the leading edge (Figures 2A and 2C). However, there was no change in lamellipodia recycling (Figure 2D). It is important to note that Tβ4 depletion did not change cellular F-actin levels (Figure 2G) or alter the rate of retrograde flow (Figure S2) relative to control cells, indicating that baseline polymerization and depolymerization of actin in the lamellipodia were similar. These results demonstrate that actin coming from the cytosolic pool and from recycled lamellipodia filaments are distinct and under different mechanisms of regulation, and these may be considered separate pathways.

Tβ4 KD Does Not Reduce the Cytoplasmic Mobility of Actin

To gain insight into the mechanism of how Tβ4 enhances localization of G-actin to the leading edge from the cytosolic pool, we investigated the mobility of cytosolic PA-GFP-actin by photoactivating PA-GFP-actin in a small region (3-μm diameter) in the cell center and simultaneously monitoring PA-GFP fluorescence at real time (30 frames per second). Surprisingly, we found that actin mobility was unchanged in the absence of Tβ4 (Figures 2E and 2F). We used shRNA against Cofilin1 (Cof1) as a positive control, as it has already been determined that Cof1 depletion causes a reduction in actin mobility (Kiuchi et al., 2007; Vitriol et al., 2013) (Figure 2F). To ensure that this was not a phenomenon specific to γ-actin, we also measured the effect of Tβ4 and Cof1 depletion on the mobility of PA-GFP-β-actin and found that the results were the same (Figure S3B). The actin mobility data implied that the role of Tβ4 in localizing actin to the leading edge is not in linking monomers to an active transport mechanism (Fan et al., 2012) but rather in enhancing their localization through diffusion and selected binding to specific regions of the lamellipodia.

G-actin that Dynamically Localizes to the Leading Edge during Membrane Protrusion Comes from the Cytosolic Pool

We then asked whether one of the two distinct sources of actin monomers we have identified specifically contributed to the dynamic population of G-actin that localizes to the leading edge during membrane protrusion. Ratiometric imaging of photoactivated GFP-actin and Lifeact-mRuby, which identifies enhanced actin monomer localization in the lamellipodia (Lee et al., 2013), determined that the band of G-actin at the cell edge is predominantly composed of actin originating from the cytosolic pool (Figures 3A and 3B). Further, we used computer vision analysis to automatically track membrane protrusions (Allen et al., 2014), allowing us to generate correlations between fluorescence intensity values and protrusion velocity. Interestingly, we found that high actin/Lifeact ratio values were exclusively found in membrane protrusions, tightly peaking in protrusions of intermediate velocity (Figure 3C). F-actin intensity increases in protrusions (Figure 3D) and peaks at velocities substantially lower than the actin/Lifeact ratio, indicating that monomer localization at the leading edge occurs after protrusion initiation. Further, we have already determined that loss of Tβ4 eliminates the high G-actin/F-actin ratio at the leading edge (Lee et al., 2013). Taken together, these results indicate that the Tβ4-regulated subset of the actin monomer pool is recruited to the lamellipodia with substantially increased rates during membrane protrusion. This also would mean that lamellipodia recycling, which is independent of Tβ4, may be used to maintain homeostasis of the constantly turning over lamellipodia and that cytosolic G-actin is recruited when an increase of filament assembly at the front is needed to push the membrane forward.

G-actin from the Cytosolic Pool Is Predominantly Targeted to Formins at the Leading Edge

When we measured the retrograde flow speed of photoactivated actin originated from either pathway, we observed a significant difference in their rates. Actin from recycled lamellipodia filaments (87.9 ± 6.2 nm/s) moved 26% faster than actin from the cytosolic pool (69.9 ± 4.1 nm/s) (Figure 4A). This indicates that actin monomers from the two distinct sources we have identified may be targeted to different types of actin filaments within the lamellipodia network. To test this, we examined the effect of inhibitors for Arp 2/3 and formins on the actin/Lifeact ratio at the leading edge, knowing that the high ratio there is derived specifically from the cytosolic pool (see previous section and Figures 3A and 3B). The Arp 2/3 complex nucleates branched actin filaments, while formins nucleate linear filaments (Chhabra and Higgs, 2007); both have been shown to have functionally distinct roles in regulating the lamellipodia actin network (Campellone and Welch, 2010), though formins also act upon Arp 2/3-derived filaments through association with growing barbed ends (Block et al., 2012). To inhibit Arp 2/3, cells were treated with 100 μM of CK-666 (Nolen et al., 2009), which is specific at this concentration (Wu et al., 2012), for

(D) Line graph showing the decrease of fluorescence at the leading edge following photoactivation of PA-GFP-actin in lamellipodia for both control (n = 12) and Tβ4 KD (n = 12) cells.
(E) A line graph showing fluorescence loss in a 3-μm circular region in the cytoplasm following photoactivation of PA-GFP-actin in both control (n = 20) and Tβ4 KD (n = 30) cells. The smaller line graph in the inset is a close-up of the time points from 0 to 1.5 s.
(F) A box-and-whisker plot showing the $t_{1/2}$ for fluorescence loss from the experiments depicted in (E), including Cof1 KD cells (n = 28) as a positive control for reduced mobility of cytoplasmic actin.
(G) A bar graph displaying the mean fluorescent intensity of control (n = 14) and Tβ4 KD (n = 15) cells that were stained with fluorescently labeled phalloidin and imaged under identical conditions.
Error bars in (B)–(E) and (G) represent 95% confidence intervals. Box-and-whisker plots denote 90th (top whisker), 75th (top edge of box), 25th (bottom edge of box), and 10th (bottom whisker) percentiles and the median (bold line in box). **$p \leq 0.01$ (Student's t test). Image scale bars are 10 μm.

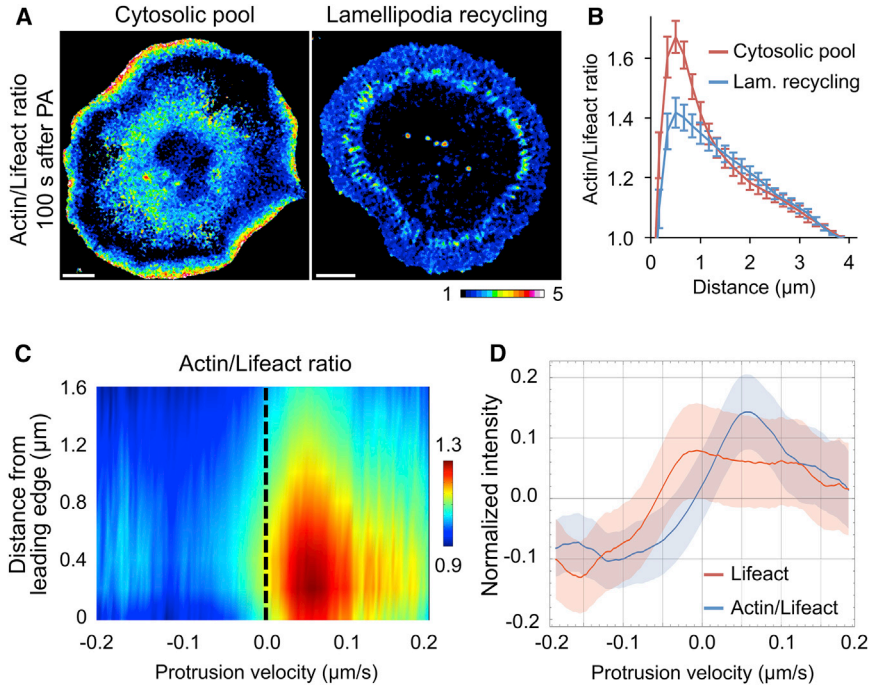

Figure 3. G-actin that Dynamically Localizes to the Leading Edge during Membrane Protrusion Comes from the Cytosolic Pool

(A) Representative ratiometric images showing the actin/Lifeact ratio (GFP-actin/Lifeact-mRuby) for cells where PA-GFP-actin was photoactivated in either the cell center (Cytosolic pool, left) or the lamellipodia (Lamellipodia recycling, right). Images were obtained 100 s after photoactivation.

(B) Line graph depicting the average actin/Lifeact ratio profile 100 s after photoactivation for cells where PA-GFP-actin was photoactivated in either the cell center (Cytosolic pool, n = 13 cells/170 line scans) or the lamellipodia (Lam. recycling n = 13 cells/279 line scans). Error bars represent 95% confidence intervals.

(C) A heatmap showing the relationship between the actin/Lifeact ratio fluorescent intensity (shown in color, scale bar at right), distance from the leading edge, and protrusion velocity. Negative velocities represent membrane retractions.

(D) A line plot of normalized fluorescence intensities 0.8 μm behind the leading edge as a function of velocity.

Error bars indicate SEM. Image scale bar, 10 μm.

10 min. The inactive analog CK-689 was used as a control. Surprisingly, while there was a dramatic shift in the composition of the lamellipodia to long bundles of parallel filaments (Figure 4B), the actin/Lifeact ratio at the leading edge was minimally reduced (Figures 4C and 4D). Furthermore, cells pre-treated with CK-666 had no problem in undergoing cell motility and localizing G-actin to the lamellipodia on the advancing side (Figure S4; Movie S5). It should be noted that CAD cells are neuronally derived (Qi et al., 1997), and Arp2/3 may be involved in, but dispensable for, their locomotion as observed in neurons (Korobova and Svitkina, 2008; Strasser et al., 2004), whereas fibroblasts require Arp2/3 for migration (Suraneni et al., 2012; Wu et al., 2012).

When cells were treated with 10 μM of the general formin inhibitor SMIFH2 (Rizvi et al., 2009) for 10 min, there was a substantial reduction in the actin/Lifeact ratio at the leading edge (Figures 4C and 4D). Strikingly, the shape of the actin/Lifeact ratio profile when formins were inhibited (Figure 4C) closely resembled the actin/Lifeact ratio profile of lamellipodia-recycled actin (Figure 3B). While there is a concern that formins exclude fluorescently labeled actin species (Chen et al., 2012), the effect in this system appears to be small since Arp2/3-depleted (and, thus, formin-dominated) lamellipodia are still efficiently labeled with EGFP-actin (Figure 4B). Further, if enhanced localization of EGFP-actin at the leading edge was caused by inefficiency in formin's ability to incorporate the labeled monomers into filaments, one would expect that the actin/Lifeact ratio would increase when Arp2/3 was inhibited and more actin was forced to be polymerized through formins. In fact, we see the opposite (Figures 4B–4D), further arguing that formin exclusion of EGFP-actin is not what is causing its enhanced localization at the leading edge. Cells treated with the formin inhibitor at this concentration were immobile, which is consistent with the idea that they are receiving G-actin that is specifically involved in membrane protrusions (Figure 3), as well as with the previous work showing a positive role for formins in regulating lamellipodia protrusions and cell migration (Block et al., 2012; Daou et al., 2014; Yang et al., 2007).

Additionally, we wanted to identify whether the reduced actin/Lifeact ratio at the leading edge in formin-depleted cells was a result of an inability to efficiently recruit actin monomers, as was the case with Tβ4- depleted cells (Figure 2). We performed experiments where we photoactivated PA-GFP-actin in the cytosolic pool and measured the rate of its incorporation into the first micron (0–1 μm) of the leading edge (Figures 4E and 4F; illustrated in Figure 1A) in the presence of the Arp 2/3 or formin inhibitor. Both treatments had a significant and nearly identical reduction on retrograde flow speed (Figure S2). While there was no change in the rate of leading-edge monomer accumulation in CK-666-treated cells (Figure 4G), there was a significant reduction in the rate of SMIFH2-treated cells relative to their respective controls (Figures 4E and 4F). In fact, that reduction in leading-edge accumulation of actin in SMIFH2-treated cells was very similar to that seen in Tβ4 KD cells. To validate that the addition of actin to the lamellipodia through formins happened exclusively at the leading edge, we also analyzed a band of the lamellipodia 2–3 μm away from the edge. While Arp2/3-inhibited cells showed a substantial decrease in actin association to the middle of the lamellipodia, formin-inhibited cells did not (Figure 4G). We propose that Tβ4-bound actin monomers are predominantly targeted to formins at the leading edge. While it has been reported that formin-mediated actin assembly occurs downstream of cellular increases in G-actin (Higashida et al., 2008, 2013), it has not been shown that these

monomers are derived from a specific subcellular pool. Future studies will be required to determine whether there are additional leading-edge actin regulators, such as Mena/VASP, that are also specifically targeted by cytosolic Tβ4/G-actin.

Tβ4 Enhances Leading-Edge G-actin Localization by Preventing It from Binding to Arp2/3 Polymerization Sites Found throughout the Lamellipodia

We used three-dimensional (3D) analysis/modeling with the Virtual Cell platform (see the Supplemental Experimental Procedures for details) to derive the diffusion rate of PA-GFP-actin. For this analysis, we used two soluble, non-polymerizable actin mutants (G13R and R62D) to account for movement of G-actin independent from filament assembly and disassembly (Figure S3A). From these data, we estimated that the diffusion coefficient of PA-GFP-actin was 3 $\mu m/s^2$ (Figure 5), which falls within the range of previously calculated diffusion coefficients for actin in cells (McGrath et al., 1998).

Then, we modified a computational model of lamellipodial actin dynamics (Smith et al., 2013) (Supplemental Experimental Procedures; Figure S5; Table S1) to simulate the effect of Tβ4 depletion (Figure 6; Movie S6). The model assumes three pools of G-actin: recycling, cytoplasmic (G_C), and bound to the membrane in complex with other proteins (G_M). Because the model reproduces the key experimental results of Figure 1 (see Figure S5), we felt that it would be an excellent way to screen for system parameters that could explain the Tβ4 KD effect. As described in previous sections, Tβ4 KD leads to a slower decay of the GFP-actin intensity at the cell center (Figure 2B) and slower recovery at the front of the lamellipodium after photoactivation of the cell middle (Figure 2C). We varied each of the model parameters individually from the control case to determine which ones can produce the shift in recovery observed experimentally. An increase in the value of the retrograde flow can modify the intensity recovery at the leading edge (Smith et al., 2013); however, we ruled out this possibility since the rate of retrograde flow does not change significantly in Tβ4 KD cells (Figure S2). Since a change in cytoplasmic mobility and, hence, a loss of active transport was also not observed in Tβ4 KD (Figure 2E), we hypothesized that the only other plausible changes in the model parameters that could potentially reproduce the experimental observations of Figures 2B–2D involved either increasing the binding rate of G_C at the back of the lamellipodium or decreasing the association rate of G_C at the leading edge. We ruled out the latter scenario by setting the rate of $G_C \rightarrow G_M$ to zero and keeping all other rate constants unchanged. These simulations produced recovery curves that substantially differed from those observed experimentally (compare Figure 6F to Figure 2C). However, by increasing the binding rate of G_C at the back of the lamellipodium (Figure 6B), we were able to reproduce all of the experimental observations from Tβ4 KD experiments where actin was photoactivated in the cell center (Figure 6D). Further, the simulated Tβ4 KD cells had about 15% less actin within 5 μm from the leading edge, as compared to the control case (Figure 6C). This is of the same order as the percent change of intensity in experiments (Figure 6G). We also monitored the intensity decay close to the leading edge in simulations of photoactivation of the whole lamellipodium (Figure 6E) to mimic the lamellipodia recycling assay and found that the results are consistent with experimental data shown in Figure 2D.

One caveat of these simulations is that they required that the diffusion coefficient of G_C be reduced by 50% in the Tβ4 KD simulations, which is in contrast to the experimental result that Tβ4 KD does not affect cytoplasmic actin mobility (Figure 2E). However, our model does not take into account that there are different types of filaments regulated by specific actin-binding proteins. In light of the experimental results that Tβ4-G-actin specifically is directed to formin-mediated filaments in the lamellipodia, it is certainly plausible that the effective diffusion coefficient of G-actin that is not in complex with Tβ4 could be locally reduced by binding more promiscuously to different types of actin within a network—in this case, to the back of the lamellipodia.

The Tβ4 KD model predicted a less sharp sigmoidal recovery at the back of the lamellipodium (Figure 6D, 2–3 μm). This loss of sigmoidal shape is due to polymerization of G_C at the back of the lamellipodium, before retrograde transports F-actin polymerized at the leading edge to this region (Smith et al., 2013). We went back to the experimental data to determine whether this hypothesis was correct. Using the same experiments from Figure 2, we re-analyzed the data by measuring a second 1-μm-wide band of the lamellipodia, this time at 2–3 μm back from the leading edge (Figure 6H). As the model predicted (Figure 6D), a significantly less sharp sigmoidal recovery was observed at the back of the lamellipodia (Figure 6I). Analysis of the data from 20 s after photoactivation—a time point at which a substantial amount of actin has localized to the leading edge but retrograde flow has not yet transported this actin to the band 2–3 μm behind the leading edge (Figure 6H)—revealed a substantial increase in the localization of cell center actin to the back of the lamellipodia. Thus, it appears that one of the roles that Tβ4 plays in localizing actin to the leading edge is to protect it from Arp2/3-mediated polymerization sites in the middle and back of the lamellipodia, ensuring that the G-actin gets delivered to formins and potentially other actin regulators, such as Mena/VASP, at the very front of lamellipodia.

DISCUSSION

In summary, we have shown that the lamellipodial F-actin networks are constructed and maintained from two distinct sub-cellular sources of G-actin. Monomers from each compartment are targeted to different actin filament sub-sets at the leading edge and have distinct functions: Tβ4-mediated G-actin localization from the cytosolic prompts formin-based actin assembly or filament elongation for membrane protrusion, whereas Tβ4-independent lamellipodia actin recycling maintains the lamellipodia steady state. Finally, we have provided evidence that the mechanism of Tβ4-enhanced actin localization at the leading edge occurs by preventing the diffusing monomers from associating with Arp2/3-mediated polymerization sites in the middle and back of the lamellipodium. Finally, the largest conceptual contribution of this article is that an actin network can be assembled from distinct monomer sources, with each contributing differently to actin spatiotemporal dynamics. It will be exciting to see if this concept remains true for

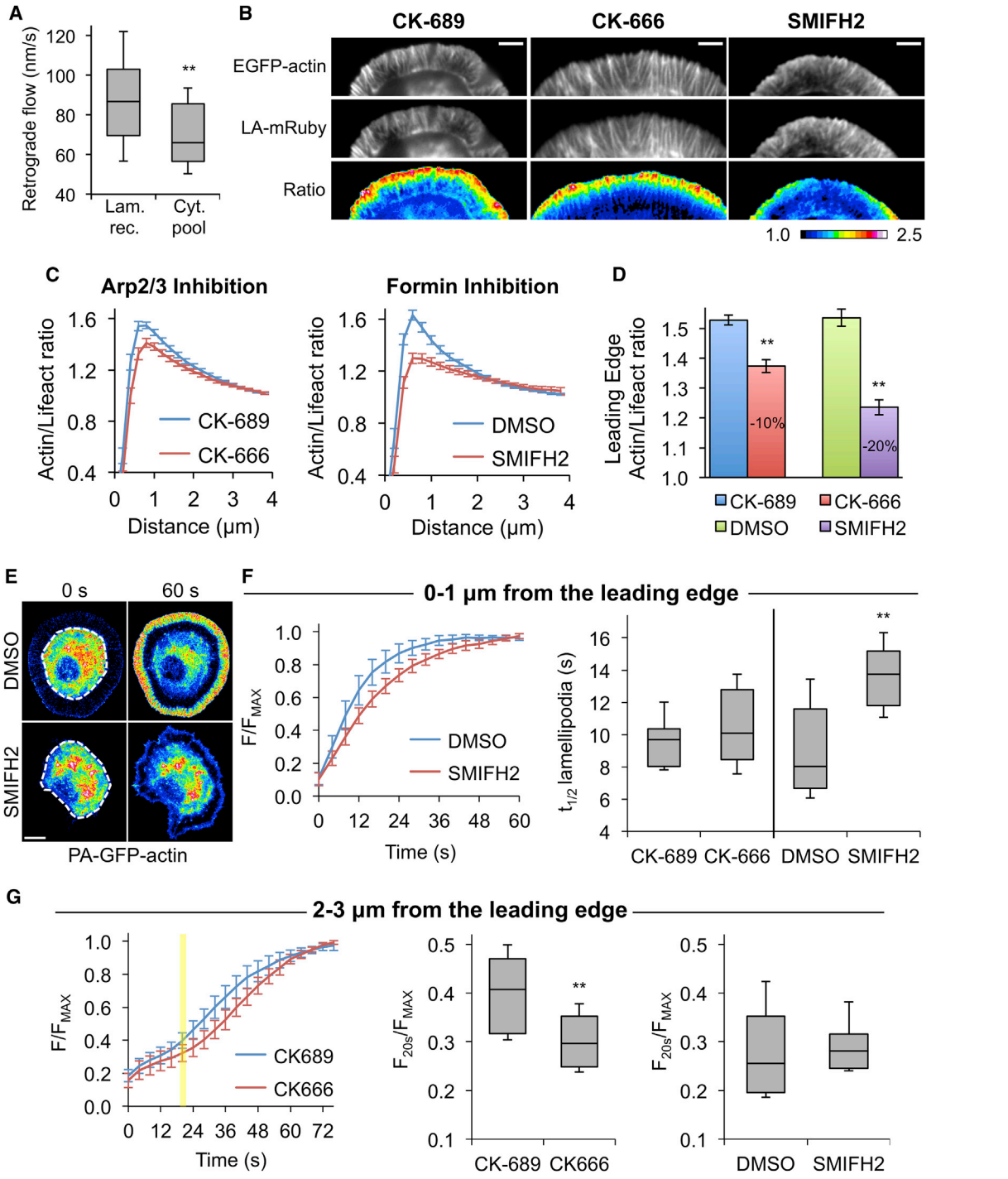

Figure 4. Actin from the Cytosolic Pool Is Primarily Targeted to Formin-Regulated Filaments

(A) Box-and-whisker plot depicts the retrograde flow rate of lamellipodia actin originating from recycled lamellipodia filaments or the cytosolic pool. Plots denote 90th (top whisker), 75th (top edge of box), 25th (bottom edge of box), and 10th (bottom whisker) percentiles and the median (bold line in box). **$p = 1 \times 10^{-6}$ (Student's t test).

(B) Representative images show EGFP-actin (top panels), Lifeact-mRuby (LA-mRuby, middle panels), and the actin/Lifeact ratio (bottom panels) for cells treated with 100 μM of the control analog of the Arp2/3 inhibitor (CK-689, left column), 100 μM of the Arp2/3 inhibitor (CK-666, middle column), or 10 μM of the formin inhibitor (SMIFH2, right column) for 10 min.

(C) Line graphs depict the average actin/Lifeact ratio profile for cells treated with CK-666 (100 μM, n = 10 cells/100 line scans), SMIFH2 (10 μM, n = 13 cells/130 line scans), and their respective controls (CK689: 100 μM, n = 14 cells/140 line scans; DMSO: 10 μM, n = 11 cells/110 line scans) for 10 min.

(legend continued on next page)

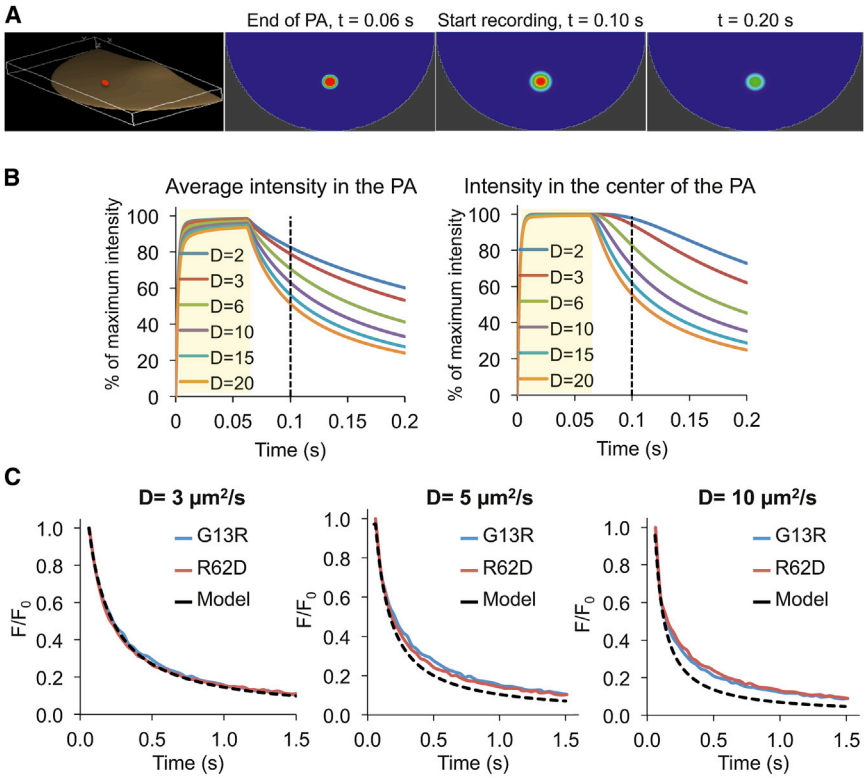

D

Diffusion rate (μm/s²)	Actin construct	RMSD (Root mean square deviation)
D=2	G13	0.0174
	R62	0.0371
D=3	G13	0.0172
	R62	0.0114
D=5	G13	0.0564
	R62	0.0396
D=10	G13	0.0779
	R62	0.0629

Figure 5. Calculation of the PA-GFP-Actin Diffusion Rate

(A) Images from the Virtual Cell model showing the 3D shape of the cell (leftmost panel), the area that is being photoactivated (in red), and a time sequence showing PA-GFP-actin fluorescence loss in a simulation where the diffusion coefficient for actin has been set to 3 μm/s^2.

(B) Line plots from simulations of varying actin diffusion coefficients showing either average intensity in the photoactivated area (PA) (left) or the intensity in the center of the photoactivated area (right). The first 0.065 s that corresponds to the time the region is being irradiated in the in vivo experiments is highlighted in yellow. Virtual Cell modeling allows us to compensate for the dissipated fluorescence during photoactivation.

(C) Line plots showing the G13R and R62 experimental data with the simulated data (model) from Virtual Cell. Simulations were run with varying PA-GFP-actin diffusion rates.

(D) Root-mean-square deviation (RMSD) analysis describing how well the fit is between the experimental (G13R and R62D) and simulated data for simulations of carrying actin diffusion coefficients. D = 3 was selected because it most accurately described both the G13R and R62D experimental data.

some, or even all, of the diverse actin structures found within the cell.

The result that Tβ4-G-actin localized to the leading edge through diffusion was somewhat surprising, since it has been recently shown in migrating endothelial cells that Tβ4 can form a complex with G-actin and Myosin 1C to deliver actin monomers to the leading edge faster than diffusion would allow (Fan et al., 2012). However, we do not see any change in cytoplasmic actin mobility when Tβ4 is depleted (Figure 2E). Thus, Myosin-1C-mediated transport may represent a type of actin delivery that is specific to endothelial cells or a specialized event in cell migration that happens in addition to diffusion-based delivery to the leading edge. In neurons, it has been estimated that approximately 50% of all ATP production goes toward maintaining dynamic actin networks (Bernstein and Bamburg, 2003). If another 15%–20% of ATP was required just to move the actin to where it needs to polymerize (Fan et al., 2012), then that leaves very little left for all of the remaining cellular processes that require ATP. From a bioenergetic standpoint, it makes sense to rely on diffusion as the principal means for actin localization when possible. We do acknowledge that the system is not far from being limited by diffusion (see the concentration gradient of G_C in Figure 6C) and that directed transport may be essential in certain cases to overcome that limitation. However, through blocking of potential binding sites on the way to its target, cytosolic Tβ4-bound G-actin can participate

(D) Bar graphs show the average actin/Lifeact ratio at the leading edge for cells treated with CK-666 (left), SMIFH2 (right), and their respective controls. **$p \leq 0.01$ (Student's t test).

(E) Pseudocolored fluorescent images of PA-GFP-actin in cells treated with 10 μM DMSO or SMIFH2 both immediately after (0 s) and 60 s after photoactivation.

(F) The line graph shows the increase in fluorescence intensity at the leading edge for DMSO- and SMIFH2-treated cells, and the box-and-whisker plot depicts the $t_{1/2}$ for fluorescence gain at the leading edge for cells treated with CK-689 (n = 11), CK-666 (n = 10), DMSO (n = 12), and SMIFH2 (n = 10) in experiments where actin was photoactivated at the cell center.

(G) The line graph shows the increase in fluorescence intensity at the middle (2–3 μm) of the lamellipodium for CK-689- and CK-666-treated cells, and the box-and-whisker plot depicts distribution of fluorescence increases for the time point 20 s after photoactivation for cells treated with CK-689 (n = 12), CK-666 (n = 11), DMSO (n = 12), and SMIFH2 (n = 7) in experiments where actin was photoactivated at the cell center.

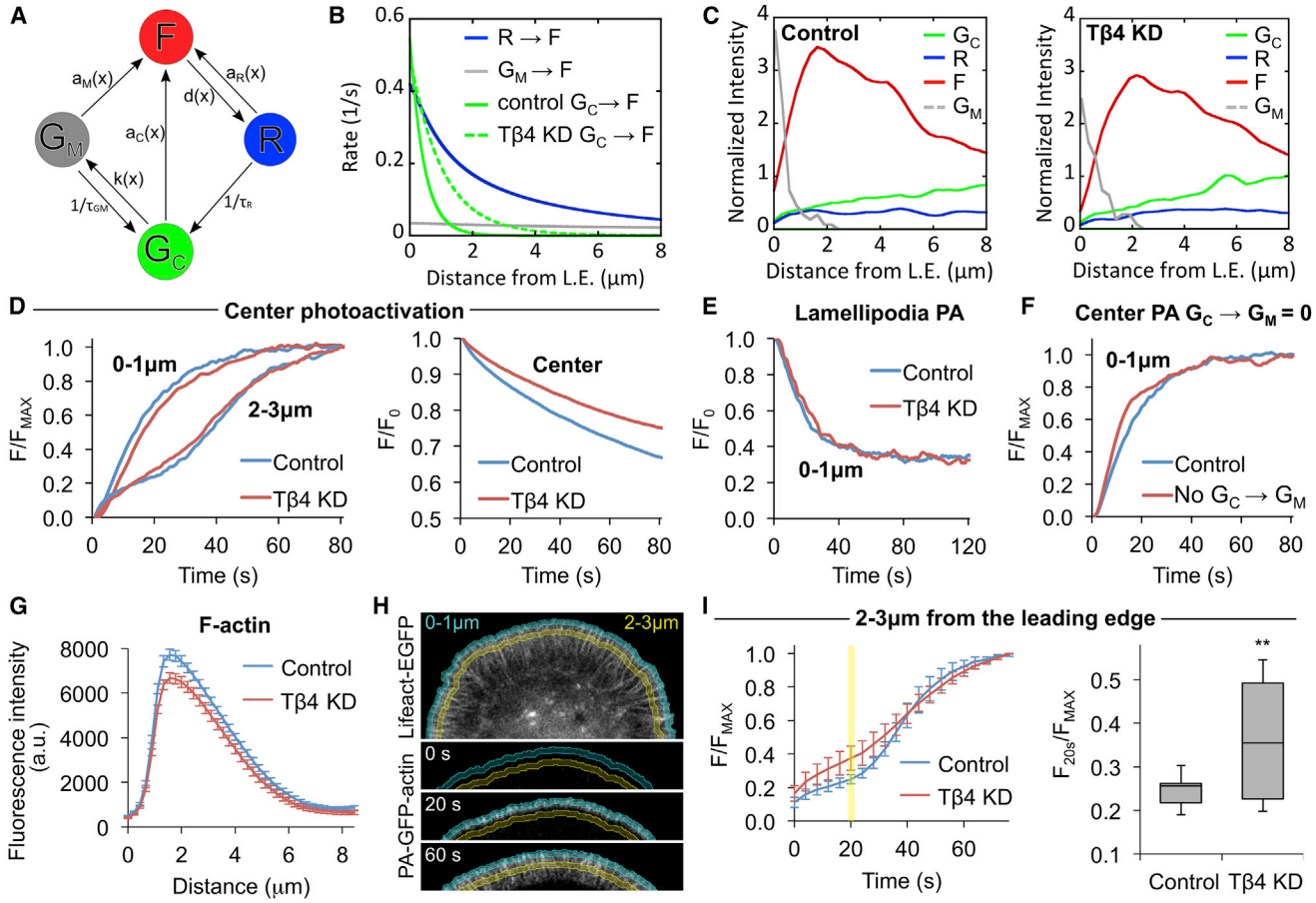

Figure 6. Simulations of PA-GFP-Actin Photoactivation Reveal Mechanism of Tβ4-Mediated Targeting of G-actin to the Leading Edge

(A) Model with three diffusing species: recycling actin (R), G_C, and G_M, shown with the rates that allow conversion between each species.

(B) Rates of R, G_M, and G_C association to F-actin as a function of distance to leading edge (L.E.). The Tβ4 KD case is simulated by assuming that G_C binds over a more extended region across the lamellipodium and has a smaller diffusion coefficient.

(C) Graph of simulated intensities at steady state normalized to the value of G_C in the center of the simulation for both control and Tβ4 KD simulation conditions. The difference in F-actin levels at the peak between control and Tβ4 KD is approximately 15%.

(D) The left graph shows an increase in simulated intensity at the lamellipodium front (0–1 μm from the leading edge) and back (2–3 μm from the leading edge) after simulated photoactivation of all particles farther than 6 μm from the front of the lamellipodium (cell center PA). The right graph depicts decay of intensity in a photoactivation simulation away from the cell center for both control and Tβ4 KD to compare with Figure 2B.

(E) Decay of intensity at the front (0–1 μm from the leading edge) in simulated images of activation of all particles within 6 μm from the leading edge (lamellipodia PA) for both control and Tβ4 KD to compare with Figure 2D.

(F) Increase in simulated intensity at the lamellipodium front (0–1 μm) as in (D), after setting the $G_C \rightarrow G_M$ rate to zero. The change in shape of the recovery curves does not match that of the Tβ4 KD in experiments in Figure 2C.

(G) A line profile of endogenous F-actin amounts in both control (16 cells, 162 line scans) and Tβ4 KD (16 cells, 161 line scans) cells. The difference between the two at the peak is approximately 15%, matching the simulated steady state for control and Tβ4 KD conditions.

(H) A depiction of the bands in the lamellipodia corresponding to 0–1 μm and 2–3 μm behind the leading edge. The top image shows Lifeact-EGFP, and the bottom panels shows selected images from a time lapse of PA-GFP-actin after it is photoactivated.

(I) The line graph on the left shows the change in intensity for the region of the lamellipodium 2–3 μm from the leading edge for control (n = 11) and Tβ4 KD (n = 17) cells. The box-and-whisker plot on the right highlights the time point at 20 s after photoactivation (noted with a yellow bar in the line graph). The box-and-whisker plots denote 90th (top whisker), 75th (top edge of box), 25th (bottom edge of box), and 10th (bottom whisker) percentiles and the median (bold line in box). $^{**}p \leq 0.01$ (Student's t test).

in fast diffusive delivery to the leading edge without the energetic burden of active transport.

Further, it appears that, at steady state, the lamellipodia is significantly supplied with recycled G-actin from F-actin disassembly at the middle and rear. While we have provided evidence that a large fraction of F-actin is recycled, we were not able to identify molecules uniquely involved in recycling. One hypothesis of how recycling would work is that the sites of polymerization are so dense where the G-actin is being created that the monomers are more likely to bind there than anywhere else, and no additional modulation of localization is needed. Another possibility is that recycling involves slowly diffusing actin

oligomers (Smith et al., 2013), which would yield a similar result. This creates an interesting concept that the lamellipodia can develop a steady state independent from external stimulation. In turn, this would mean that only lamellipodia protrusions downstream of extracellular or intracellular cues require an additional supply of actin to promote specific types of network assembly needed to push the membrane forward. This is supported by our previous findings that depletion of Tβ4 does not affect the ability of the cell to assemble a lamellipodia (Lee et al., 2013). Further, the lamellipodia of Tβ4 KD cells are the same size (Lee et al., 2013), have the same rates of retrograde flow (Figure S2), and have only a modest reduction in the amount of total F-actin (Figure 5G) as control lamellipodia. Thus, the lamellipodia steady state is relatively unchanged. However, Tβ4 KD lamellipodia have severe defects in their ability to sustain a membrane protrusion, which ultimately result in axon guidance defects (Lee et al., 2013). It will be interesting to determine the complete molecular pathway that governs G-actin recruitment to the leading edge in future experiments.

The most likely candidate for a binding partner that helps Tβ4-bound G-actin specifically interact with formins at the leading edge is Profilin. Profilin is regulated by extracellular cues in cell motility, localizes to the cell membrane at the leading edge, and is the known delivery agent of G-actin for formins and Mena/VASP (Ding et al., 2012). Further, Profilin can form a tertiary complex with Tβ4 and actin (Yarmola et al., 2001), and depletion of Profilin1 causes a significant decrease in the enhanced localization of G-actin to the leading edge but does not eliminate it completely (Lee et al., 2013). The implication of this hypothesis is that either Profilin is present at the leading edge sans actin, where it waits to accept monomers from Tβ4 before handing them off to formins, or that Profilin is forming a complex with Tβ4/G-actin somewhere on its journey from the cytosol and they arrive at the leading edge together. It has been shown that the leading edge is where Tβ4 becomes dissociated from actin (Fan et al., 2009), though the role of Profilin in this process is unclear. More experiments are required to identify Profilin's involvement and whether there are additional layers of specificity in Tβ4-mediated actin delivery to the leading edge.

EXPERIMENTAL PROCEDURES

DNA Constructs

The following additional DNA constructs were used in this study: Lifeact-mRuby (pN1-Lifeact-mRuby, provided by Roland Wedlich-Soldner, Max-Planck Institute of Biochemistry), PA-GFP-actin (pC1 PA-GFP-γ-actin), PA-GFP-actin$_{G13R}$ (pC1 PA-GFP-γ-actin$_{G13R}$), PA-GFP-actin$_{R62D}$ (pC1 PA-GFP-γ-actin$_{R62D}$), PA-GFP-β-actin (pC1 PA-GFP-β-actin), and EGFP-γ-actin (pCS2+-GFP-γ-actin). DNA constructs were prepared using the GenElute HP Endotoxin-Free Plasmid Maxiprep Kit (Sigma-Aldrich).

CAD Cell Culture

CAD cells were cultured in DMEM/F12 medium (GIBCO) supplemented with 8% fetal calf serum, 1% L-glutamine, and 1% penicillin-streptomycin. They were imaged in DMEM/F12 medium without phenol red (GIBCO), supplemented with 15 mM HEPES. CAD cells were plated on coverslips coated with 10 μg/ml laminin (Sigma). After 90 min, normal culture medium was exchanged for imaging medium. CAD cells were transfected 12–24 hr prior to imaging with the appropriate constructs using X-tremeGene HP (Roche) according to manufacturer's instructions.

For short hairpin RNAi (shRNAi) knockdown, cells were infected with lentiviral particles (Santa Cruz Biotechnology) that expressed both an shRNA hairpin and a gene for puromycin resistance. Infection was done in the presence of 5 μg/ml polybrene (Santa Cruz Biotechnology). At 48 hr after infection, cells were selected with 10 μg/ml puromycin (Santa Cruz Biotechnology). This concentration was chosen because it killed 100% of uninfected cells within 24 hr. After selection, cells were continuously cultured in media containing 10 μg/ml puromycin, except during imaging experiments. Quantification of Tβ4 and Cof1 knockdown has been previously described (Lee et al., 2013; Vitriol et al., 2013).

For pharmacologic inhibition of Arp 2/3, cells were treated with 100 μM of the Arp 2/3 inhibitor CK-666 or its control analog CK-689 (EMD Millipore). For pharmacologic inhibition of formins, cells were treated with 10 μM of the Formin FH2 Domain Inhibitor SMIFH2 (EMD Millipore) or DMSO alone. To determine the actin/Lifeact ratio in these cells, they were fixed with 4% paraformaldehyde in 4% paraformaldehyde in Kreb's S buffer (145 mM NaCl, 5 mM KCl, 1.2 mM $CaCl_2$, 1.3 mM $MgCl_2$, 1.2 mM NaH_2PO_4, 10 mM glucose, 20 mM HEPES, and 0.4 M sucrose) after a 10-min incubation with the pharmacologic agent. Notably, the cells in the control and experimental groups were from the same batch of transfected cells, and all imaging was performed on the same day with identical imaging conditions.

Microscopy

Photoactivation experiments were performed on a Nikon A1R laser scanning confocal microscope equipped with an automated z-drive with Perfect Focus, multiple laser lines with AOTF control, motorized x-y stage, a second resonance scanner for high-speed imaging and photoactivation, an attached cage incubator with CO_2 and temperature control, and multiple photomultiplier tube detectors. Cells were mounted in a custom live-cell chamber. All experiments were performed using a 60× 1.49 NA PlanApoN TIRF oil immersion objective. Photoactivation of PA-GFP was performed with the 405-nm laser line (laser power 100%, 2.2-μs pixel dwell time) by irradiating a customized region (for each cell and experiment type) with a single 100-ms pulse. The power of the 405-nm laser line coming out of the objective at 100% power was approximately 1 mW.

To obtain data about the mobility of actin in the cytosol, PA-GFP-actin was photoactivated with the resonance scanner of the Nikon A1R microscope, which allowed for the simultaneous photoactivation with the 405-nm laser line (a single 65-ms pulse, 100% laser power) and monitoring of GFP channel at 30 frames per second with the 488-nm laser line. To maximize imaging speed, a 55-μm-long and 3.5-μm-tall rectangular region of the field of view was used for imaging, and the scanning direction was set to bidirectional. The photoactivation ROI was a 3-μm-diameter circle.

Imaging of the actin/Lifeact ratio following treatment of cells with CK-666, SMIFH2, and their respective controls was performed on a Nikon Eclipse Ti inverted microscope equipped with a Hamamatsu ORCA-Flash 4.0 V2 camera using a 60× 1.49 NA PlanApoN TIRF oil immersion objective. For live experiments, cells were mounted in a custom live-cell chamber and maintained at 37°C with a heated stage adaptor (Werner).

Image Analysis

Image analysis was performed with Nikon Elements and ImageJ software and exported into Microsoft Excel for analysis. To measure fluorescence intensity specifically at the leading edge, a binary region was generated by thresholding the fluorescence intensity of the Lifeact-mRuby channel in Nikon Elements so that it contained the entire cell. An erosion filter was applied to this region so that the resulting region was eroded 1 μm inward. The eroded region was then subtracted from the first binary region to generate a custom ROI that contained only the first 1 μm of the cell edge (see Movie S4 for an example). Regions of the cell that did not contain lamellipodia were excluded from the analysis.

To measure changes in PA-GFP-actin fluorescence, intensity values were background-subtracted and normalized to the time point immediately

after photoactivation. Double exponential curve fitting was performed on the fluorescence decay curves with a free online curve fitting application (previously available at http://ZunZun.com) so that the halftime, $t_{1/2}$, could be obtained.

To determine retrograde flow rates, kymographs were drawn at the edge of cells where PA-GFP-actin incorporation into the lamellipodia was clearly visible. Kymographs were drawn in as many regions of the cell as possible. Retrograde flow was measured by calculating the slope of a diagonal line that traced the rearward flow of incorporated PA-GFP-actin, representing the distance the actin traveled over time.

The actin/Lifeact ratio was generated as previously described (Lee et al., 2013). To generate edge profiles of the actin/Lifeact ratio, lines were drawn perpendicular to the cell edge, and then they were averaged and normalized to the lowest intensity value of the line.

Automated Cell Edge Velocity and Intensity Analysis

Background-corrected ratio images and the corresponding Lifeact images were used for velocity analysis. Intensity as a function of cell edge velocity was analyzed from nine cell movies having a minimum of 80 consecutive frames (~16.6 s between frames; minimum of 22-min duration). Line scans with a depth of 6 μm and a 6 μm/s maximum velocity were performed using a freely available MATLAB software package (Allen et al., 2014), with parameters set to default values. Cell boundaries for F-actin images were obtained from their corresponding ratio images. Intensity values for both ratio images as well as the f-actin channel were quantified at a depth of 0.8 μm from the edge and smoothed with a ten-point moving average. Additionally, the data were normalized to the intensity of the maximum negative velocity.

Additional experimental procedures can be found in the Supplemental Experimental Procedures.

SUPPLEMENTAL INFORMATION

Supplemental Information includes Supplemental Experimental Procedures, five figures, one table, and six movies and can be found with this article online at http://dx.doi.org/10.1016/j.celrep.2015.03.033.

AUTHOR CONTRIBUTIONS

E.A.V. designed and performed the experiments, analyzed data, and wrote the manuscript. L.M.M. and D.V. developed the computational model of PA-GFP-actin dynamics and performed analysis on that data. M.K. determined the diffusion rate of PA-GFP-actin. S.M.G. performed the computer vision analysis of membrane protrusions and the actin/Lifeact ratio. J.Q.Z. helped design the study and write the manuscript.

ACKNOWLEDGMENTS

We would like to thank Dr. Oskar Laur of the Custom Cloning Core Facility for generating the actin constructs used in this study. We thank Dr. Matthew Smith (Medical Research Council/University College London) for help with the computational modeling. We thank Dr. James Bear, Dr. Richard Cheney, and Dr. Ken Jacobson (University of North Carolina at Chapel Hill) for helpful and insightful discussions about the project. This project was supported in part by a Ruth L. Kirschstein National Research Service Award (F32NS077612) and a Pathway to Independence award (K99NS087104) from the NIH to E.A.V.; NIH (GM078994) and National Science Foundation (DMS-1200535) grants to M.K.; NIH grant R01GM098430 to L.M.M. and D.V.; NIH grant R01GM083889 to J.Q.Z.; and a National Institute of Neurological Disorders and Stroke core facilities grant (P30NS055077) to the Integrated Cellular Imaging Microscopy Core of Emory Neuroscience.

Received: February 6, 2014
Revised: November 20, 2014
Accepted: March 13, 2015
Published: April 9, 2015

REFERENCES

Allen, R.J., Tsygankov, D., Zawistowski, J.S., Elston, T.C., and Hahn, K.M. (2014). Automated line scan analysis to quantify biosensor activity at the cell edge. Methods *66*, 162–167.

Bernstein, B.W., and Bamburg, J.R. (2003). Actin-ATP hydrolysis is a major energy drain for neurons. J. Neurosci. *23*, 1–6.

Blanchoin, L., Boujemaa-Paterski, R., Sykes, C., and Plastino, J. (2014). Actin dynamics, architecture, and mechanics in cell motility. Physiol. Rev. *94*, 235–263.

Block, J., Breitsprecher, D., Kuhn, S., Winterhoff, M., Kage, F., Geffers, R., Duwe, P., Rohn, J.L., Baum, B., Brakebusch, C., et al. (2012). FMNL2 drives actin-based protrusion and migration downstream of Cdc42. Curr. Biol. *22*, 1005–1012.

Burnette, D.T., Manley, S., Sengupta, P., Sougrat, R., Davidson, M.W., Kachar, B., and Lippincott-Schwartz, J. (2011). A role for actin arcs in the leading-edge advance of migrating cells. Nat. Cell Biol. *13*, 371–381.

Campellone, K.G., and Welch, M.D. (2010). A nucleator arms race: cellular control of actin assembly. Nat. Rev. Mol. Cell Biol. *11*, 237–251.

Chen, Q., Nag, S., and Pollard, T.D. (2012). Formins filter modified actin subunits during processive elongation. J. Struct. Biol. *177*, 32–39.

Chhabra, E.S., and Higgs, H.N. (2007). The many faces of actin: matching assembly factors with cellular structures. Nat. Cell Biol. *9*, 1110–1121.

Daou, P., Hasan, S., Breitsprecher, D., Baudelet, E., Camoin, L., Audebert, S., Goode, B.L., and Badache, A. (2014). Essential and nonredundant roles for Diaphanous formins in cortical microtubule capture and directed cell migration. Mol. Biol. Cell *25*, 658–668.

Ding, Z., Bae, Y.H., and Roy, P. (2012). Molecular insights on context-specific role of profilin-1 in cell migration. Cell Adhes. Migr. *6*, 442–449.

Fan, Y., Gong, Y., Ghosh, P.K., Graham, L.M., and Fox, P.L. (2009). Spatial coordination of actin polymerization and ILK-Akt2 activity during endothelial cell migration. Dev. Cell *16*, 661–674.

Fan, Y., Eswarappa, S.M., Hitomi, M., and Fox, P.L. (2012). Myo1c facilitates G-actin transport to the leading edge of migrating endothelial cells. J. Cell Biol. *198*, 47–55.

Higashida, C., Suetsugu, S., Tsuji, T., Monypenny, J., Narumiya, S., and Watanabe, N. (2008). G-actin regulates rapid induction of actin nucleation by mDia1 to restore cellular actin polymers. J. Cell Sci. *121*, 3403–3412.

Higashida, C., Kiuchi, T., Akiba, Y., Mizuno, H., Maruoka, M., Narumiya, S., Mizuno, K., and Watanabe, N. (2013). F- and G-actin homeostasis regulates mechanosensitive actin nucleation by formins. Nat. Cell Biol. *15*, 395–405.

Kiuchi, T., Ohashi, K., Kurita, S., and Mizuno, K. (2007). Cofilin promotes stimulus-induced lamellipodium formation by generating an abundant supply of actin monomers. J. Cell Biol. *177*, 465–476.

Kiuchi, T., Nagai, T., Ohashi, K., and Mizuno, K. (2011). Measurements of spatiotemporal changes in G-actin concentration reveal its effect on stimulus-induced actin assembly and lamellipodium extension. J. Cell Biol. *193*, 365–380.

Korobova, F., and Svitkina, T. (2008). Arp2/3 complex is important for filopodia formation, growth cone motility, and neuritogenesis in neuronal cells. Mol. Biol. Cell *19*, 1561–1574.

Lai, F.P., Szczodrak, M., Block, J., Faix, J., Breitsprecher, D., Mannherz, H.G., Stradal, T.E., Dunn, G.A., Small, J.V., and Rottner, K. (2008). Arp2/3 complex interactions and actin network turnover in lamellipodia. EMBO J. *27*, 982–992.

Lee, C.W., Vitriol, E.A., Shim, S., Wise, A.L., Velayutham, R.P., and Zheng, J.Q. (2013). Dynamic localization of G-actin during membrane protrusion in neuronal motility. Curr. Biol. *23*, 1046–1056.

McGrath, J.L., Tardy, Y., Dewey, C.F., Jr., Meister, J.J., and Hartwig, J.H. (1998). Simultaneous measurements of actin filament turnover, filament fraction, and monomer diffusion in endothelial cells. Biophys. J. *75*, 2070–2078.

Nolen, B.J., Tomasevic, N., Russell, A., Pierce, D.W., Jia, Z., McCormick, C.D., Hartman, J., Sakowicz, R., and Pollard, T.D. (2009). Characterization of two

classes of small molecule inhibitors of Arp2/3 complex. Nature *460*, 1031–1034.

Pollard, T.D., and Borisy, G.G. (2003). Cellular motility driven by assembly and disassembly of actin filaments. Cell *112*, 453–465.

Pollard, T.D., Blanchoin, L., and Mullins, R.D. (2000). Molecular mechanisms controlling actin filament dynamics in nonmuscle cells. Annu. Rev. Biophys. Biomol. Struct. *29*, 545–576.

Qi, Y., Wang, J.K., McMillian, M., and Chikaraishi, D.M. (1997). Characterization of a CNS cell line, CAD, in which morphological differentiation is initiated by serum deprivation. J. Neurosci. *17*, 1217–1225.

Riedl, J., Crevenna, A.H., Kessenbrock, K., Yu, J.H., Neukirchen, D., Bista, M., Bradke, F., Jenne, D., Holak, T.A., Werb, Z., et al. (2008). Lifeact: a versatile marker to visualize F-actin. Nat. Methods *5*, 605–607.

Rizvi, S.A., Neidt, E.M., Cui, J., Feiger, Z., Skau, C.T., Gardel, M.L., Kozmin, S.A., and Kovar, D.R. (2009). Identification and characterization of a small molecule inhibitor of formin-mediated actin assembly. Chem. Biol. *16*, 1158–1168.

Smith, M.B., Kiuchi, T., Watanabe, N., and Vavylonis, D. (2013). Distributed actin turnover in the lamellipodium and FRAP kinetics. Biophys. J. *104*, 247–257.

Strasser, G.A., Rahim, N.A., VanderWaal, K.E., Gertler, F.B., and Lanier, L.M. (2004). Arp2/3 is a negative regulator of growth cone translocation. Neuron *43*, 81–94.

Suraneni, P., Rubinstein, B., Unruh, J.R., Durnin, M., Hanein, D., and Li, R. (2012). The Arp2/3 complex is required for lamellipodia extension and directional fibroblast cell migration. J. Cell Biol. *197*, 239–251.

Svitkina, T.M. (2013). Ultrastructure of protrusive actin filament arrays. Curr. Opin. Cell Biol. *25*, 574–581.

Vitriol, E.A., Wise, A.L., Berginski, M.E., Bamburg, J.R., and Zheng, J.Q. (2013). Instantaneous inactivation of cofilin reveals its function of F-actin disassembly in lamellipodia. Mol. Biol. Cell *24*, 2238–2247.

Wu, C., Asokan, S.B., Berginski, M.E., Haynes, E.M., Sharpless, N.E., Griffith, J.D., Gomez, S.M., and Bear, J.E. (2012). Arp2/3 is critical for lamellipodia and response to extracellular matrix cues but is dispensable for chemotaxis. Cell *148*, 973–987.

Yang, C., Czech, L., Gerboth, S., Kojima, S., Scita, G., and Svitkina, T. (2007). Novel roles of formin mDia2 in lamellipodia and filopodia formation in motile cells. PLoS Biol. *5*, e317.

Yarmola, E.G., Parikh, S., and Bubb, M.R. (2001). Formation and implications of a ternary complex of profilin, thymosin beta 4, and actin. J. Biol. Chem. *276*, 45555–45563.

Zicha, D., Dobbie, I.M., Holt, M.R., Monypenny, J., Soong, D.Y., Gray, C., and Dunn, G.A. (2003). Rapid actin transport during cell protrusion. Science *300*, 142–145.